Метод автоматизированной обработки научных публикаций

Хвостова М.О.[a], Артамонов А.А.[b], Пряхина Д.И.[c]

[a] Филиал Московского государственного университета имени М.В. Ломоносова в городе Дубне
[b] Национальный исследовательский ядерный университет «МИФИ»
[c] Объединенный институт ядерных исследований

Актуальность исследования

Увеличение объёма научных публикаций в мире.

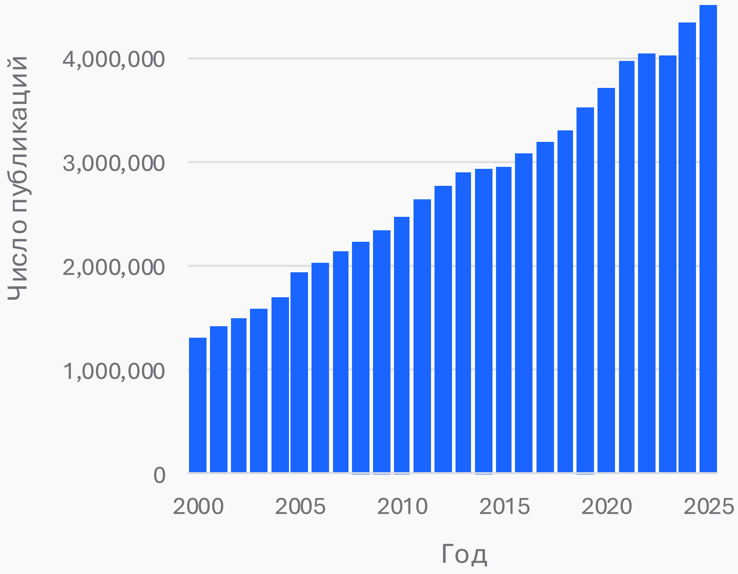

https://www.scimagojr.com/worldreport.php (01.07.2026)

Разнообразие журналов по различным научным направлениям.

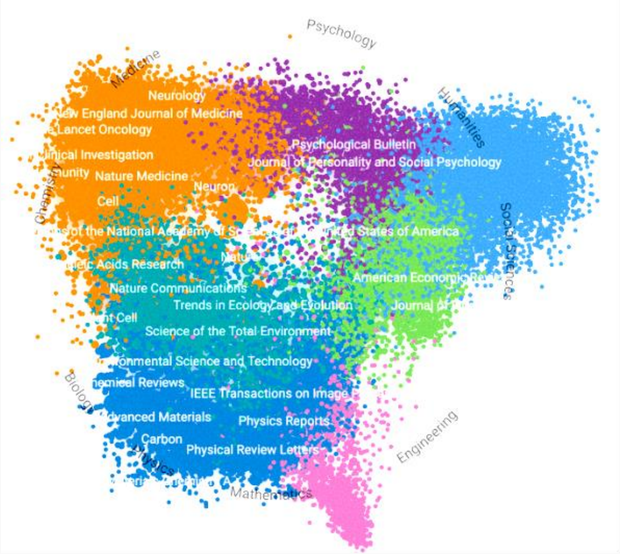

https://www.scimagojr.com/shapeofscience/ (01.07.2026)

Проблемы необработанных данных

Большой объём и неструктурированность.

Избыточность для целевых исследовательских запросов.

Неравномерность распределения «полезной» информации.

Цель работы

Автоматизация обработки научных публикаций для формирования структурированных представлений целевых данных.

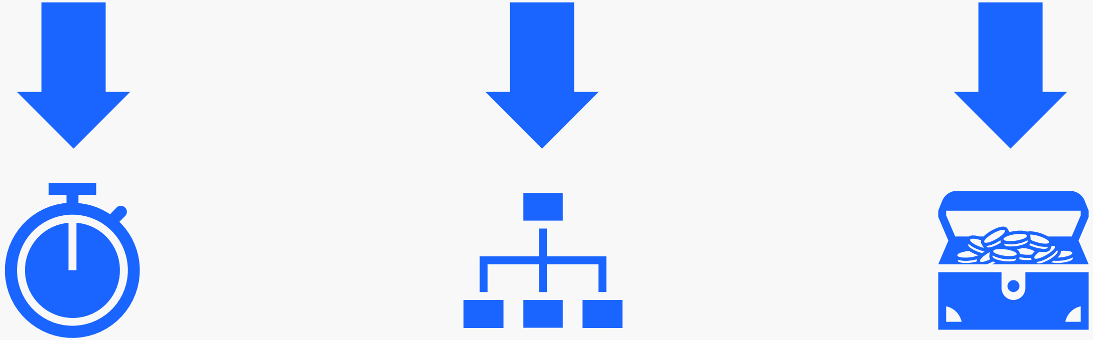

Скорость обработки

Удобство обращения

Компактность представления

Предложенный метод

Распознавание текстовых, табличных и графических образов с помощью машинного обучения и эвристик.

смысловая связь

АКТАНТ [1] — **СИРКОНСТАНТ** [1]

Эксперимент

Опытный образец

Испытуемый

Время

Место

Продукт

Физическое свойство

Параметр среды

Инструмент

Предложенный метод

Блок-схема обработки научной публикации.

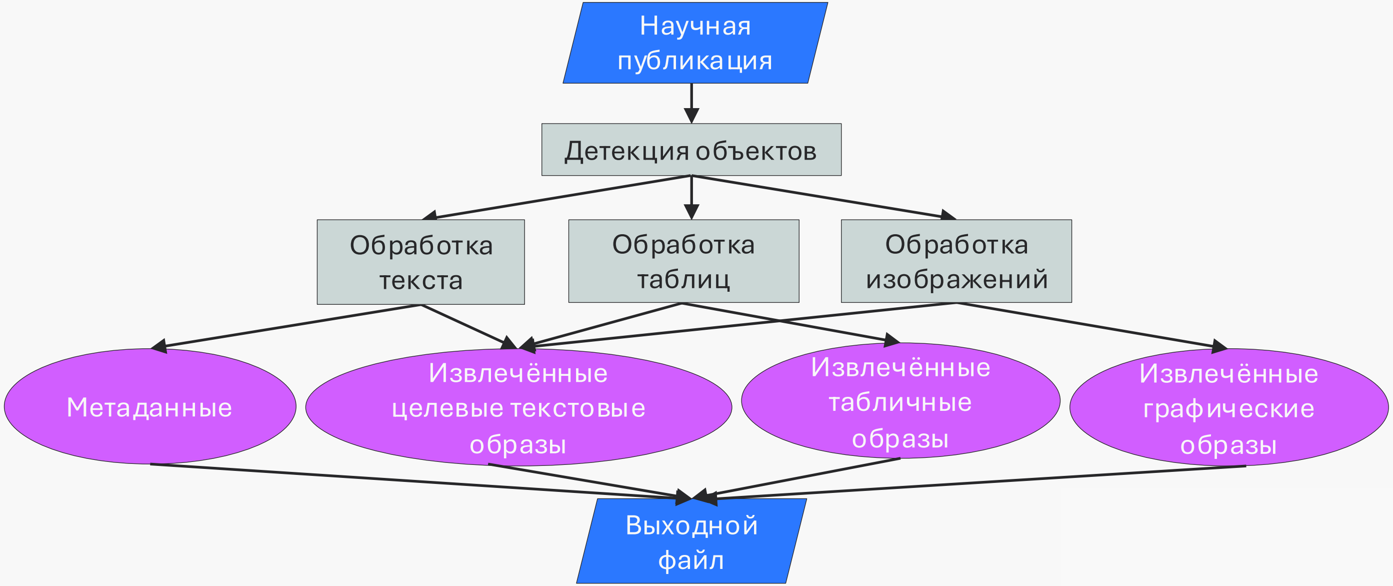

Распознавание текстовых образов

Блок-схема обработки текста.

E.g.:
“Fusion of 48Ti + 58Fe and 58Ni + 54Fe below the Coulomb barrier”;
10.1103/physrevc.92.064607

E.g.:
pulsed beams of 48Ti;
a metallic 40Ca target;
the stainless steel AISI 304.

E.g.:
at the INFN Laboratori Nazionali di Legnaro (LNL, Italy);
the three bombarding energies (300, 450 and 600 MeV);
collimated silicon detectors.

Продукционные правила

Необходимы для формирования и связывания актантов и сирконстантов.

"The reaction layer thickness of the highstrength aluminum alloy AA 6082 is 50 µm."

Правило: [DET] → [compound/amod/nummod]+ → [NOUN/PROPN] → [prep/punct]*
Разбор: [the] → [reaction layer] → [thickness] → [of]

Правило: [NUM]+ → [unit_pattern]*
Разбор: [50] → [µm]

Правило: [именная группа] → [VERB/AUX] → [числовая группа]
Разбор: [the reaction layer thickness] → [is] → [50 µm]

Сирконстант: (the reaction layer thickness, 50 µm).

Актант: (the highstrength aluminum alloy AA 6082).

Распознавание табличных образов

Блок-схема обработки таблицы.

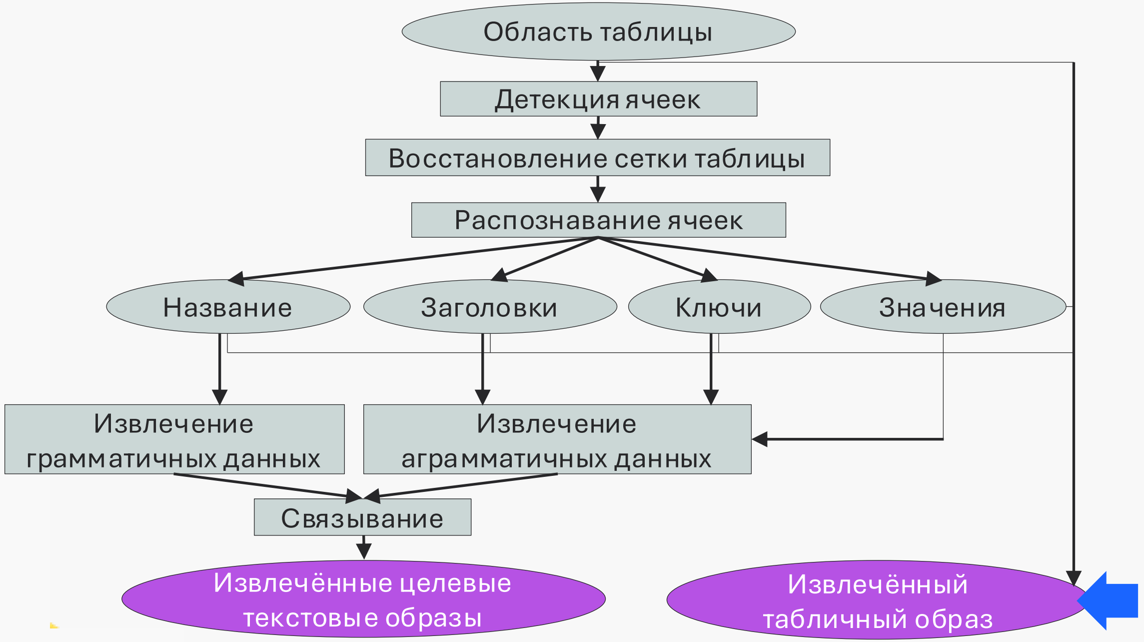

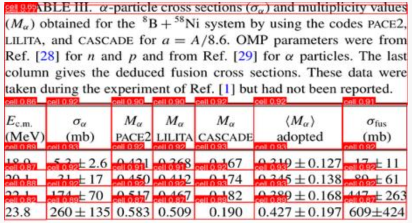

[illegible]ABLE III. α-particle cross sections (σ_α) and multiplicity values (M_α) obtained for the $^8B + ^{58}Ni$ system by using the codes PACE2, LILITA, and CASCADE for $a = A/8.6$. OMP parameters were from Ref. [28] for n and p and from Ref. [29] for α particles. The last column gives the deduced fusion cross sections. These data were taken during the experiment of Ref. [1] but had not been reported.

$E_{c.m.}$ (MeV)	σ_α (mb)	M_α PACE2	M_α LILITA	M_α CASCADE	$\langle M_\alpha \rangle$ adopted	σ_{fus} (mb)
[illegible]	[illegible] ± 2.6	[illegible]	[illegible]	[illegible]67	[illegible] ± 0.127	[illegible] ± 11
[illegible]	[illegible] ± 17	[illegible]	[illegible]	[illegible]74	[illegible] ± 0.138	[illegible] ± 61
[illegible]	[illegible] ± 70	[illegible]	[illegible]	[illegible]82	[illegible] ± 0.168	[illegible] ± 263
23.8	260 ± 135	0.583	0.509	0.190	0.427 ± 0.197	609±424

TABLE III. α-particle cross sections (σα) and multiplicity values (Mα) obtained for the e 8B + 58Ni system by using the codes PACE2, LILITA, and CAsCADE for a = A/8.6. OMP parameters were from Ref. [28] for n and p and from Ref. [29] for α particles. The last column gives the deduced fusion cross sections. These data were taken during the experiment of Ref. [1] but had not been reported.

[[" (MeV)", "σα (mb)", "Mα PACE2", "Mα LILITA", "Mα CASCADE", "(Mα) adopted", "Ofus (mb)"],
["18.9", "5.3±2.6", "0.421", "0.368", "0.167", "0.319±0.127", "17±11"],
["20.1", "31±17", "0.45", "0.412", "0.174", "0.345±0.138", "89±61"],
["22.1", "174±70", "0.517", "0.467", "0.182", "0.389±0.168", "447±263"],
["23.8", "260±135", "0.583", "0.509", "0.19", "0.427±0.197", "609±424"]]

Распознавание графических образов

Блок-схема обработки изображения.

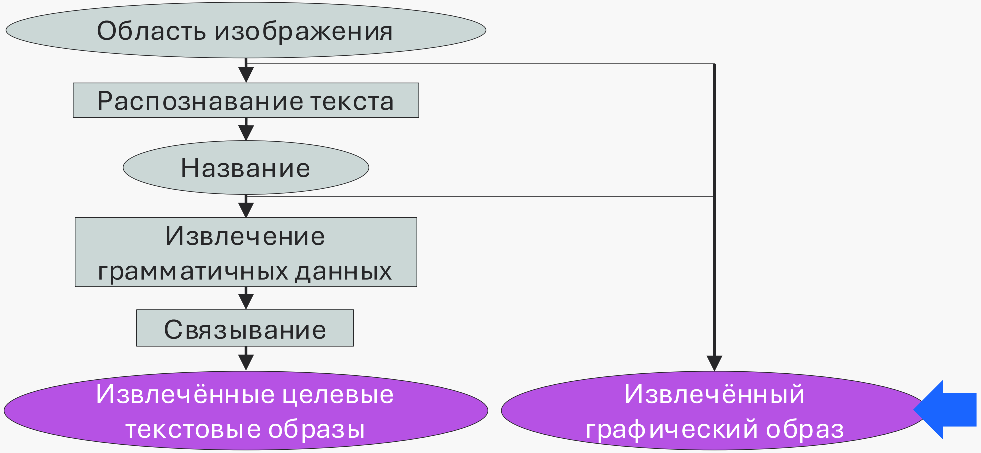

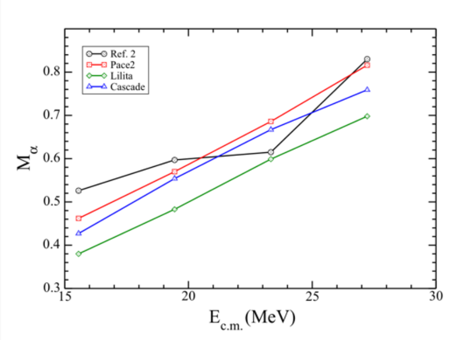

FIG. 4. α-particle multiplicities for the $^{8}B + ^{28}Si$ system calculated with several different evaporation codes. The Ref. [2] values are calculated from the "R values" given in Ref. [30] using the formula $M_\alpha = (R+1)^{-1}$.

FIG. 4. α-particle multiplicities for the ^{8}B + 28Si system calcu- lated with several different evaporation codes. The Ref. [2] values are calculated from the "R values' given in Ref. [30] using the formula Mα = (R + 1)−1.

Метрики качества

Полнота и точность извлечения с пороговой близостью на основе взвешенного редакционного расстояния.

$$\mathrm{sim}(a,b) = 1 - \frac{W(a,b)}{\mathrm{max\_dist}},$$

$$W(i,j) = \min \begin{cases} W(i-1,j) + w_{\mathrm{del}} \\ W(i,j-1) + w_{\mathrm{ins}} \\ W(i-1,j-1) + w_{\mathrm{rep}}(a_i,b_j) \end{cases}$$

$$w_{\mathrm{rep}}(a_i,b_j) = \begin{cases} 0.0, & a_i = b_j \\ 0.5, & \text{символы оптически похожи} \\ 1.0, & \text{иначе} \end{cases}$$

$$\mathrm{max\_dist} = \max(|a|,|b|) \times 1.0$$

$$\textbf{Precision} = \frac{Found\ correct \mid sim(a,b) \geq \tau}{Found\ correct \mid sim(a,b) \geq \tau\ + Found\ incorrect}$$

$$\textbf{Recall} = \frac{Found\ corect \mid sim(a,b) \geq \tau}{All\ correct}$$

a – эталонная строка,
b – извлечённая строка,
τ – пороговое значение.

Апробация

Формирование базы данных свойств припоев[3, 4, 5] кафедры №9 «Физические проблемы материаловедения» МИФИ

Инструменты: регулярные выражения.

Наполнение базы знаний NRV[2] Лаборатории ядерных реакций ОИЯИ.

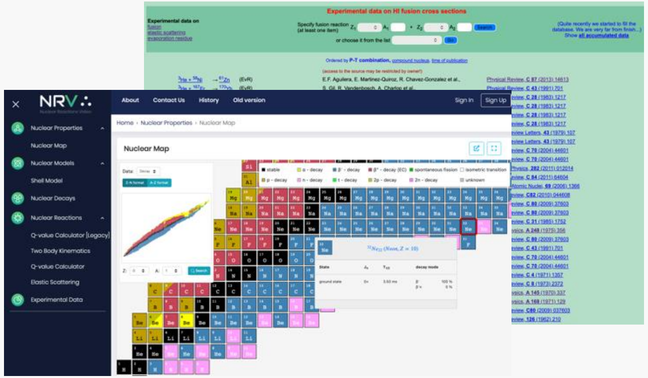

Инструменты: CNN, лингвистический анализатор, LLM, регулярные выражения.

Апробация

Тестирование: 3 публикации (физика низких энергий).

"Fusion of 48Ti + 58Fe and 58Ni + 54Fe below the Coulomb barrier" [6]

"Deformation effects on sub-barrier fusion cross sections in 16O + 174,176Yb." [7]

"Above-barrier fusion enhancement of proton-halo systems" [8]

Валидация таблиц: 40 публикаций (смешанная тематика).

Пороговая близость $\tau = 0.9$

Образ	N	Recall	Precision
Title	3	1	1
Author	40	0.9	1
Ref	3	1	1
DOI	3	1	1
Setup	4	1	1
Beam	3	1	1
Target	5	1	1
Detected particle	5	1	1
Detector	7	1	1
Accuracy	5	1	1
Table cell	6717	98.2	98.2
Figure title	17	1	1
Figure image	17	1	1

Заключение

Рост объёма и разнообразия научных публикаций и их гетерогенность (текст, таблицы, графика) требуют перехода от ручного анализа к автоматизированной фильтрации, структурированию и семантическому сжатию.

Эффективное извлечение фактологической информации возможно при гибридном подходе, сочетающем компьютерное зрение, лингвистический анализ и машинное обучение.

Предложенный подход формализует научный факт через связи между его участниками, преобразуя неструктурированный текст в структурированные данные, что ведет к переходу от систем текстового поиска к интерпретируемым базам знаний.

Источники

[1] Tesnière L. Éléments de syntaxe structurale. — Paris : Klincksieck, 1959. — 670 p.
[2] Denikin, A. S., Alekseev, A. P., Zagrebaev, V. I. et al. (2016). NRV web knowledge base on low-energy nuclear physics. Physics of Atomic Nuclei, 79(5). https://doi.org/10.1134/S1063778816040141
[3] Khvostova M., Abramov A., Artamonov A. Solder Alloys Data Mining for Materials Research // Physics of Elementary Particles and Atomic Nuclei. – 2026. – Vol. 57, № 4.
[4] Хвостова М.О., Абрамов А.В., Артамонов А.А., Сучков А.Н. Программная обработка полнотекстовых научных публикаций для формирования тематических баз данных свойств материалов // Цифровое материаловедение : Сборник статей II Всероссийской научно-практической конференции. – М. : Изд-во МГТУ им. Н.Э. Баумана, 2025. – С. 140–144.
[5] Хвостова М.О., Абрамов А.В., Артамонов А.А., Сучков А.Н. Цифровая платформа консолидации знаний о припоях для решения прикладных и исследовательских задач современного материаловедения // Русский инженер : Сборник тезисов II Всероссийского конгресса с международным участием. – М. : Изд-во МГТУ им. Н.Э. Баумана, 2024. – С. 207–209.
[6]
[7]
[8]

Спасибо за внимание!

Программная реализация

Инструмент	Характеристики
PicoDet_layout_1x	CPU: 12.77-26.96 мс, GPU: 6.75-9.62 мс, Хранилище: 7.4 МБ [22, 23].
RT-DETR-L_wireless_table_cell_det	CPU: 256.56-402.55 мс, GPU: 27.02-33.42 мс, Хранилище: 124 МБ [22, 24].
PP-LCNet_x1_0_doc_ori	CPU: 1.19-3.24 мс, GPU: 0.59-2.62 мс, Хранилище: 7 МБ [22, 25].
PP-OCRv5_mobile_det	CPU: 28.58-51.00 мс, GPU: 3.13-8.79 мс, Хранилище: 4.7 МБ [22, 26].
PP-LCNet_x1_0_textline_ori	CPU: 2.98 мс, GPU: - мс, Хранилище: 6.5 МБ [15, 18].
PP-OCRv5_mobile_rec	CPU: 1.46-5.43 мс, GPU: 5.32-21.20 мс, Хранилище: 16 МБ [22, 26].
Qwen3-0.6B	0.6 млрд параметров, контекст ~33 тыс. токенов; RAM: ~8.5 ГБ, Хранилище: 1.52 ГБ [27, 28].

Итого: Хранилище: 1.69 ГБ

Пример вывода

{
"title": "Deformation effects on sub-barrier fusion cross sections in 16O + 174,176Yb",
"authors": [
"Tapan Rajbongshi", "K. Kalita", "S. Nath", "J. Gehlot",
"Tathagata Banerjee", "Ish Mukul", "R. Dubey", "N. Madhavan", "C. J. Lin",
"M. Shareef", "Neeraj Kumar", "P. Jisha", "P. Sharma"
],
"affiliations": [
"Nuclear Physics Group, Inter University Accelerator Centre, Aruna Asaf Ali Marg, New Delhi 110067, India", "Department of Physics, Gauhati University, Guwahati 781014, India", ...],
"reference": "Physical Review C 93 (2016)",
"doi": "10.1103/physrevc.93.054622",
"setup": "15 UD Pelletron accelerator facility",
"beam": "16O",
"targets": ["174Yb", "176Yb"],
"detectors": ["silicon detectors"],
"accuracy": null,
"detected_particles": ["γ photons", "neutrons", "light charged particles"]
}

PHYSICAL REVIEW C **93**, 054622 (2016)

Deformation effects on sub-barrier fusion cross sections in $^{16}O + ^{174,176}Yb$

Tapan Rajbongshi,[1] K. Kalita,[1,*] S. Nath,[2] J. Gehlot,[2] Tathagata Banerjee,[2] Ish Mukul,[3] R. Dubey,[2] N. Madhavan,[2] C. J. Lin,[4] A. Shamlath,[5] P. V. Laveen,[5] M. Shareef,[5] Neeraj Kumar,[6] P. Jisha,[7] and P. Sharma[8]

[1] *Department of Physics, Gauhati University, Guwahati 781014, India*
[2] *Nuclear Physics Group, Inter University Accelerator Centre, Aruna Asaf Ali Marg, New Delhi 110067, India*
[3] *Department of Particle Physics and Astrophysics, Weizmann Institute of Science, Rehovot 76100, Israel*
[4] *China Institute of Atomic Energy, P. O. Box 275(10), Beijing 102413, People's Republic of China*
[5] *Department of Physics, School of Mathematical and Physical Sciences, Central University of Kerala, Kasaragod 671328, India*
[6] *Department of Physics and Astrophysics, University of Delhi, Delhi 110007, India*
[7] *Department of Physics, University of Calicut, Calicut 673635, India*
[8] *Department of Physics, Panjab University, Chandigarh 160014, India*

(Received 3 February 2016; revised manuscript received 5 April 2016; published 25 May 2016)

Background: Couplings with various reaction channels are known to enhance sub-barrier fusion cross sections by several orders in magnitude. However, a few open questions still remain. For example, the influence of higher order static deformations on sub-barrier fusion cross sections is yet to be comprehensively understood.
Purpose: We study the role of hexadecapole nuclear deformation effect on sub-barrier fusion cross sections. Also, this work aims to extract hexadecapole deformation (β_4) in nuclei in the lanthanide region.
Method: The evaporation residue (ER) excitation functions for $^{16}O + ^{174,176}Yb$ were measured at laboratory beam energies (E_{lab}) in the range of 64.6–103.6 MeV. Measurements were carried out by employing the recoil mass spectrometer Heavy Ion Reaction Analyzer (HIRA) at IUAC, New Delhi. Fusion barrier distributions (BDs) were extracted from data. Results from the experiment were subjected to coupled-channels analysis, in which β_4 was varied as a free parameter.
Results: Experimental fusion cross sections at energies below the barrier expectedly showed strong enhancement compared to the predictions from the one-dimensional barrier penetration model. Data were satisfactorily reproduced after inclusion of negative β_4 for both the targets in the coupled-channels calculation.
Conclusions: The significant role of hexadecapole deformation was observed in the sub-barrier fusion of $^{16}O + ^{174,176}Yb$. The proposed value of β_4 reproduced the measured fusion excitation function reasonably well. The BDs from these data were also extracted but no definitive conclusions could be drawn from them.

DOI: 10.1103/PhysRevC.93.054622

I. INTRODUCTION

Heavy ion-induced fusion reactions around the Coulomb barrier have been pursued quite intensely for the past few decades [1–4]. Fusion cross sections are found to be enhanced, in some cases by several orders of magnitude, over the prediction from the one-dimensional barrier penetration model near and below the Coulomb barrier [5,6]. The coupling of internal degrees of freedom such as transfer of valence neutrons, neck formation, zero point motion, and static deformation have been considered in order to explain observed enhancements of the fusion cross sections. The coupling with intrinsic degrees of freedom has an effect of changing the height of the barrier. Barriers lower than the one-dimensional Coulomb barrier are then responsible for the enhancement of fusion cross sections.

Deformation of one or both the reaction partners is known to enhance sub-barrier fusion cross sections [7–10]. The extent to which a particular degree of freedom (e.g., quadrupole or hexadecapole deformation) contributes to the sub-barrier fusion enhancement independently can be estimated by calculating the asymptotic energy shift [11] associated with that particular degree of freedom [12–14]. Besides, the idea that a positive β_4 could enhance sub-barrier fusion cross sections more, in comparison to what a negative β_4 does, was put forward for the reaction $^{16}O + ^{186}W$ [15]. On the other hand, due to negative hexadecapole deformations, enhancements of sub-barrier fusion cross sections have been measured for the reactions ^{16}O on $^{176,180}Hf$ and $^{182,184,186}W$ by Leigh *et al.* [16]. Also the same conclusion was drawn theoretically for the $^{16}O + ^{184}W$ system [17].

The barrier distributions (BDs) are known to be highly sensitive to higher order nuclear deformations. The experimental BDs can be obtained from the fusion cross sections [2,18] as well as from quasielastic scattering data [19,20]. The shapes of the experimental BDs extracted from the fusion excitation functions [9] for $^{16}O + ^{154}Sm$ and $^{16}O + ^{186}W$ reveal that the role of positive and negative β_4 is evident in the qualitative differences between the two BDs.

We performed an experiment to measure ER excitation functions for the systems $^{16}O + ^{174,176}Yb$ forming compound nuclei (CN) $^{190,192}Pt$ near and below the Coulomb barrier. Since ^{16}O is a doubly magic spherical nucleus, effects of nuclear shapes on fusion cross sections are expected to be solely due to target nuclei. We investigated the role of β_4 in reproducing fusion data with the help of coupled-channels (CC) calculations. The experimental details are described in Sec. II while analysis of data and results are presented in Sec. III. We summarize our work and conclude in Sec. IV.

*ku_kalita@yahoo.com

https://journals.aps.org/prc/abstract/10.1103/PhysRevC.93.054622

PicoDet_layout_1x

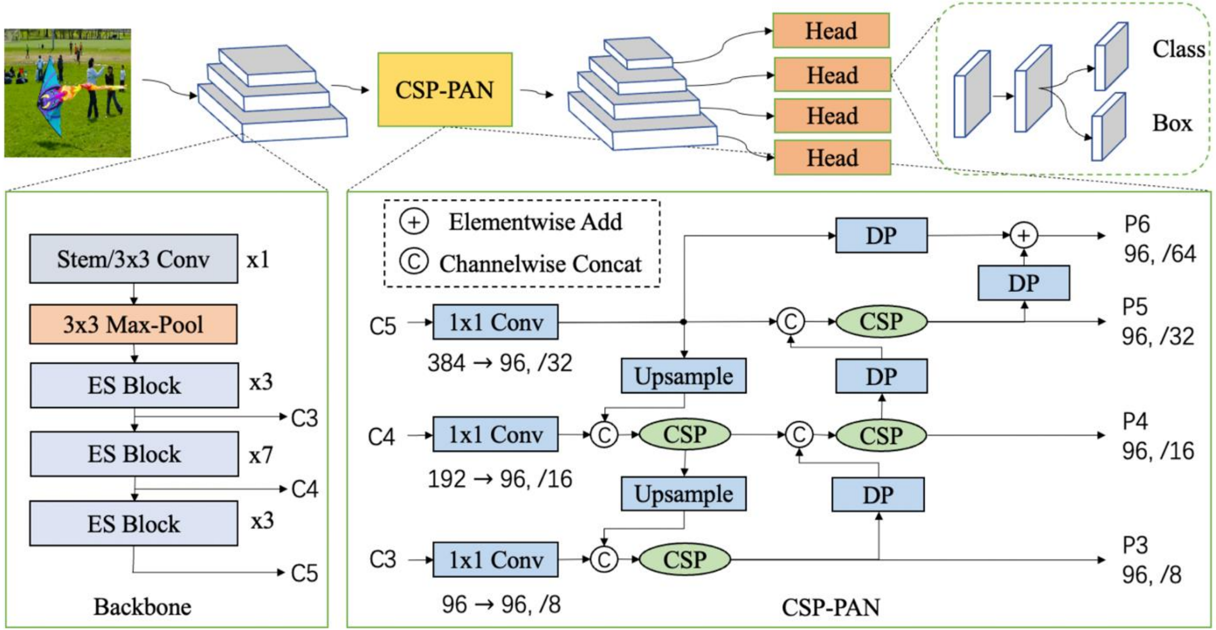

Figure 2. PP-PicoDet Architecture. The Backbone is ESNet, which outputs C3-C5 feature maps to the neck. The neck is CSP-PAN, which inputs three feature maps and outputs four feature maps. For PP-PicoDet-S, the input channel numbers are [96, 192, 384], and the output channel numbers are [96, 96, 96, 96]. DP module uses depthwise and pointwise convolution.

Yu, G., et al. (2021). PP-PicoDet: A Better Real-Time Object Detector on Mobile Devices. arXiv. https://doi.org/10.48550/arXiv.2111.00902.
https://paddlepaddle.github.io/PaddleX/latest/en/support_list/models_list.html#text-line-orientation-classification-module (дата обращения: 16.03.2026).

PicoDet_layout_1x

Model	Size	Params(M)	FLOPs(G)	mAP(0.5:0.95)	mAP(0.5)	Latency(ms)
YOLOv3-Tiny	416	8.86	5.62	16.6	33.1	25.42
YOLOv4-Tiny	416	6.06	6.96	21.7	40.2	23.69
MobileDet-CPU	320	3.85	1.02	24.2	-	-
YOLObile	320	4.59	3.59	31.6	49.0	-
PP-YOLO-Tiny	320	1.08	0.58	20.6	-	6.75
PP-YOLO-Tiny	416	1.08	1.02	22.7	-	10.48
NanoDet-M	320	0.95	0.72	20.6	-	8.71
NanoDet-M	416	0.95	1.2	23.5	-	13.35
NanoDet-M-1.5x	416	2.08	2.42	26.8	-	15.83
YOLOX-Nano	416	0.91	1.08	25.8	-	19.23
YOLOX-Tiny	416	5.06	6.45	32.8	-	32.77
YOLOv5n	640	1.9	4.5	28.4	46.0	40.35
YOLOv5s	640	7.2	16.5	37.2	56.0	78.05
PP-PicoDet-ShuffleNetV2	416	1.17	1.53	30.0	44.6	15.06 | **10.63***
PP-PicoDet-MV3-large-1x	416	3.55	2.80	35.6	52.0	20.71 | **17.88***
PP-PicoDet-LCNet-1.5x	416	3.10	3.85	36.3	52.2	21.29 | **20.8***
PP-PicoDet-S	320	0.99	0.73	**27.1**	**41.4**	8.13 | **6.65***
PP-PicoDet-S	416	0.99	1.24	**30.6**	**45.5**	12.37 | **9.82***
PP-PicoDet-M	416	2.15	2.50	**34.3**	**49.8**	17.39 | **15.88***
PP-PicoDet-L	640	3.30	8.91	**40.9**	**57.6**	54.11 | **50.55***

Table 1. Comparison of the speed and accuracy of different lightweight detectors on COCO *val*. We use the NCNN[42] library for latency testing and add Paddle Lite[43] inference latency(Marked as *) for the PP-PicoDet model. The latency of all models tested on Qualcomm Snapdragon® 865(4*A77+4*A55) Processor with batch size of 1 and CPU threads of 4.

Yu, G., et al. (2021). PP-PicoDet: A Better Real-Time Object Detector on Mobile Devices. arXiv. https://doi.org/10.48550/arXiv.2111.00902.
https://paddlepaddle.github.io/PaddleX/latest/en/support_list/models_list.html#text-line-orientation-classification-module (дата обращения: 16.03.2026).

RT-DETR-L_wireless_table_cell_det

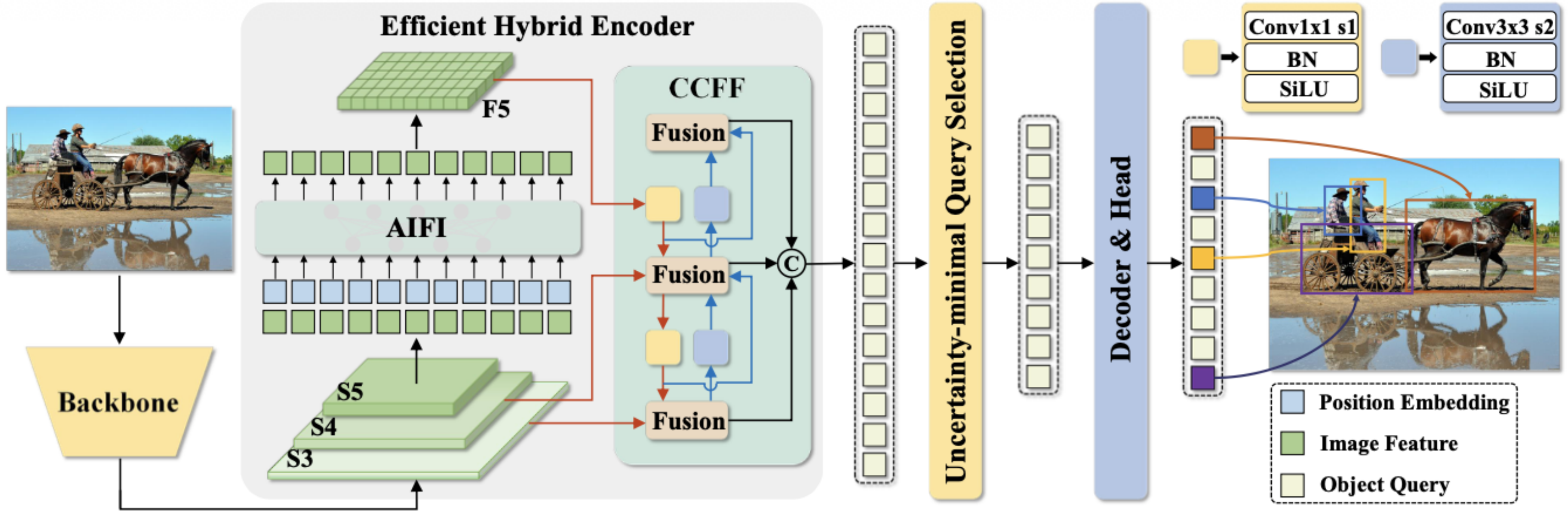

Figure 4. Overview of RT-DETR. We feed the features from the last three stages of the backbone into the encoder. The efficient hybrid encoder transforms multi-scale features into a sequence of image features through the Attention-based Intra-scale Feature Interaction (AIFI) and the CNN-based Cross-scale Feature Fusion (CCFF). Then, the uncertainty-minimal query selection selects a fixed number of encoder features to serve as initial object queries for the decoder. Finally, the decoder with auxiliary prediction heads iteratively optimizes object queries to generate categories and boxes.

Zhao, Y., et al. (2024). DETRs Beat YOLOs on Real-time Object Detection. arXiv. https://doi.org/10.48550/arXiv.2304.08069.

RT-DETR-L_wireless_table_cell_det

Model	Backbone	#Epochs	#Params (M)	GFLOPs	$FPS_{bs=1}$	AP^{val}	AP^{val}_{50}	AP^{val}_{75}	AP^{val}_{S}	AP^{val}_{M}	AP^{val}_{L}
Real-time Object Detectors											
YOLOv5-L [11]	-	300	46	109	54	49.0	67.3	-	-	-	-
YOLOv5-X [11]	-	300	86	205	43	50.7	68.9	-	-	-	-
PPYOLOE-L [40]	-	300	52	110	94	51.4	68.9	55.6	31.4	55.3	66.1
PPYOLOE-X [40]	-	300	98	206	60	52.3	69.9	56.5	33.3	56.3	66.4
YOLOv6-L [16]	-	300	59	150	99	52.8	70.3	57.7	34.4	58.1	70.1
YOLOv7-L [38]	-	300	36	104	55	51.2	69.7	55.5	35.2	55.9	66.7
YOLOv7-X [38]	-	300	71	189	45	52.9	71.1	57.4	36.9	57.7	68.6
YOLOv8-L [12]	-	-	43	165	71	52.9	69.8	57.5	35.3	58.3	69.8
YOLOv8-X [12]	-	-	68	257	50	53.9	71.0	58.7	35.7	59.3	70.7
End-to-end Object Detectors											
DETR-DC5 [4]	R50	500	41	187	-	43.3	63.1	45.9	22.5	47.3	61.1
DETR-DC5 [4]	R101	500	60	253	-	44.9	64.7	47.7	23.7	49.5	62.3
Anchor-DETR-DC5 [39]	R50	50	39	172	-	44.2	64.7	47.5	24.7	48.2	60.6
Anchor-DETR-DC5 [39]	R101	50	-	-	-	45.1	65.7	48.8	25.8	49.4	61.6
Conditional-DETR-DC5 [27]	R50	108	44	195	-	45.1	65.4	48.5	25.3	49.0	62.2
Conditional-DETR-DC5 [27]	R101	108	63	262	-	45.9	66.8	49.5	27.2	50.3	63.3
Efficient-DETR [42]	R50	36	35	210	-	45.1	63.1	49.1	28.3	48.4	59.0
Efficient-DETR [42]	R101	36	54	289	-	45.7	64.1	49.5	28.2	49.1	60.2
SMCA-DETR [9]	R50	108	40	152	-	45.6	65.5	49.1	25.9	49.3	62.6
SMCA-DETR [9]	R101	108	58	218	-	46.3	66.6	50.2	27.2	50.5	63.2
Deformable-DETR [45]	R50	50	40	173	-	46.2	65.2	50.0	28.8	49.2	61.7
DAB-Deformable-DETR [23]	R50	50	48	195	-	46.9	66.0	50.8	30.1	50.4	62.5
DAB-Deformable-DETR++ [23]	R50	50	47	-	-	48.7	67.2	53.0	31.4	51.6	63.9
DN-Deformable-DETR [17]	R50	50	48	195	-	48.6	67.4	52.7	31.0	52.0	63.7
DN-Deformable-DETR++ [17]	R50	50	47	-	-	49.5	67.6	53.8	31.3	52.6	65.4
DINO-Deformable-DETR [44]	R50	36	47	279	5	50.9	69.0	55.3	34.6	54.1	64.6
Real-time End-to-end Object Detector (ours)											
RT-DETR	R50	72	42	136	**108**	**53.1**	**71.3**	**57.7**	34.8	58.0	70.0
RT-DETR	R101	72	76	259	**74**	**54.3**	**72.7**	58.6	36.0	58.8	**72.1**

Table 2. Comparison with SOTA (only L and X models of YOLO detectors, see Appendix for the comparison with S and M models). We do not test the speed of other DETRs, except for DINO-Deformable-DETR [44] for comparison, as they are not real-time detectors. Our RT-DETR outperforms the state-of-the-art YOLO detectors and DETRs in both speed and accuracy.

Zhao, Y., et al. (2024). DETRs Beat YOLOs on Real-time Object Detection. arXiv. https://doi.org/10.48550/arXiv.2304.08069.

PP-LCNet_x1_0

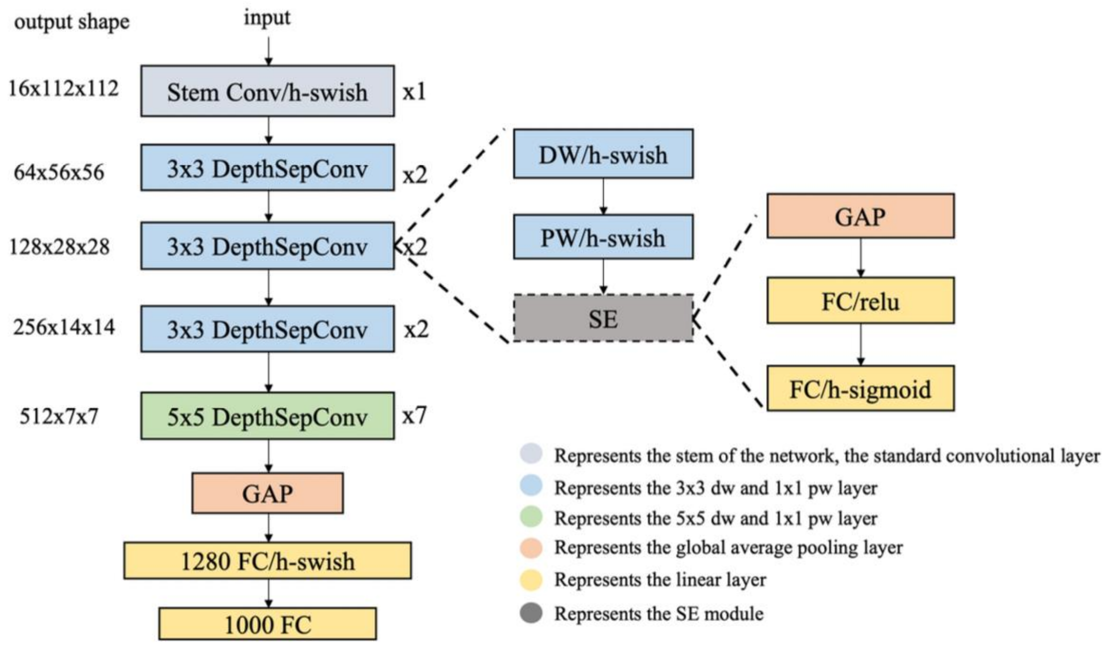

Figure 2. A detailed view of PP-LCNet. The dotted box represents optional modules.The stem part uses standard 3 × 3 convolution. DepthSepConv means depth-wise separable convolutions, DW means depth-wise convolution, PW means point-wise convolution, GAP means Global Average Pooling.

Cui, C., et al. (2021). PP-LCNet: A Lightweight CPU Convolutional Neural Network. arXiv. https://doi.org/10.48550/arXiv.2109.15099.

PP-LCNet_x1_0

Model	Params(M)	FLOPs(M)	Top-1 Acc.(%)	Top-5 Acc.(%)	Latency(ms)
MobileNetV2-0.25x	1.5	34	53.21	76.52	2.47
MobileNetV3-small-0.35x	1.7	15	53.03	76.37	3.02
ShuffleNetV2-0.33x	0.6	24	53.73	77.05	4.30
PP-LCNet-0.25x	**1.5**	**18**	**51.86**	**75.65**	**1.74**
MobileNetV2-0.5x	2.0	99	65.03	85.72	2.85
MobileNetV3-large-0.35x	2.1	41	64.32	85.46	3.68
ShuffleNetV2-0.5x	1.4	43	60.32	82.26	4.65
PP-LCNet-0.5x	**1.9**	**47**	**63.14**	**84.66**	**2.05**
MobileNetV1-1x	4.3	578	70.99	89.68	3.38
MobileNetV2-1x	3.5	327	72.15	90.65	4.26
MobileNetV3-small-1.25x	3.6	100	70.67	89.51	3.95
ShuffleNetV2-1.5x	3.5	301	71.63	90.15	-
PP-LCNet-1x	**3.0**	**161**	**71.32**	**90.03**	**2.46**

Table 3. Comparison of state-of-the-art light networks over classification accuracy. Latency tested on Intel® Xeon® Gold 6148 Processor with batch size of 1 and MKLDNN enabled, the number of thread is 10.

Cui, C., et al. (2021). PP-LCNet: A Lightweight CPU Convolutional Neural Network. arXiv. https://doi.org/10.48550/arXiv.2109.15099.

PP-OCRv5

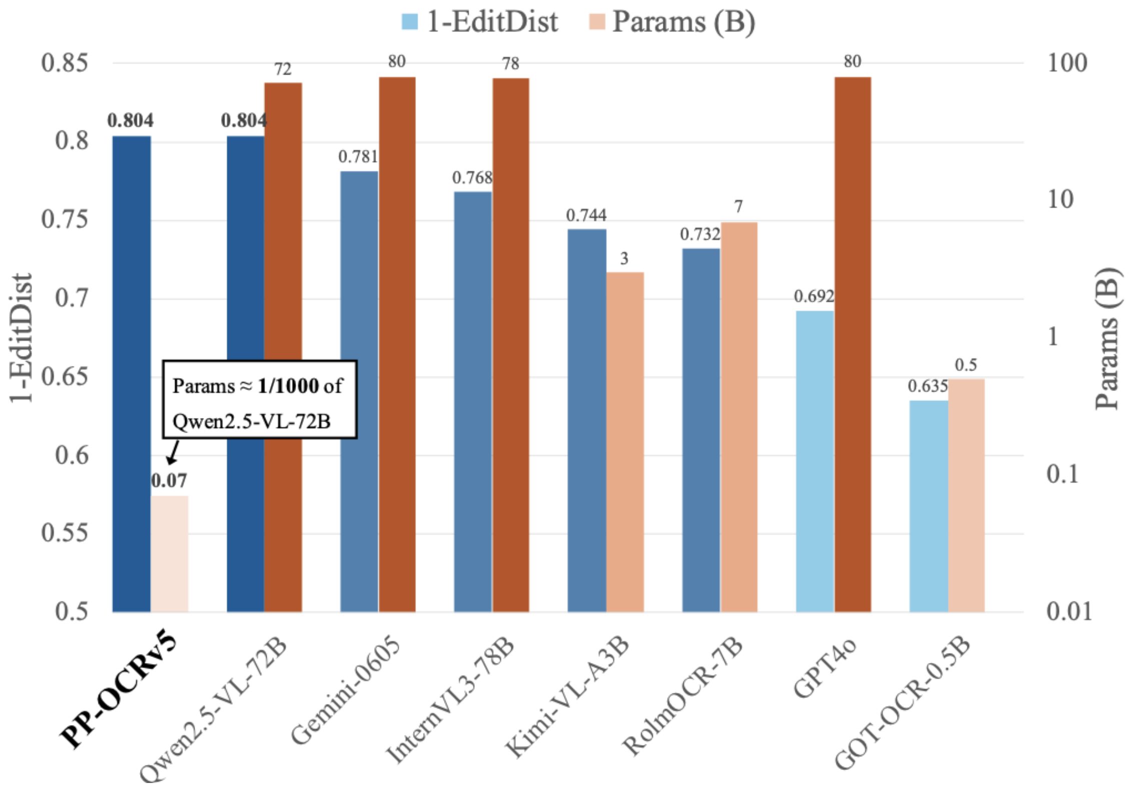

Cui, C., et al. (2021). PP-LCNet: A Lightweight CPU Convolutional Neural Network. arXiv. https://doi.org/10.48550/arXiv.2109.15099.

Qwen3-0.6

Table 19: **Comparison among Qwen3-1.7B / Qwen3-0.6B (Thinking) and other reasoning baselines. The highest and second-best scores are shown in bold and underlined, respectively.**

		DeepSeek-R1 -Distill-Qwen-1.5B	DeepSeek-R1 -Distill-Llama-8B	Qwen3-0.6B	Qwen3-1.7B
	Architecture	Dense	Dense	Dense	Dense
	# Activated Params	1.5B	8B	0.6B	1.7B
	# Total Params	1.5B	8B	0.6B	1.7B
General Tasks	MMLU-Redux	45.4	66.4	55.6	**73.9**
	GPQA-Diamond	33.8	**49.0**	27.9	40.1
	C-Eval	27.1	50.4	50.4	**68.1**
	LiveBench 2024-11-25	24.9	40.6	30.3	**51.1**
Alignment Tasks	IFEval strict prompt	39.9	59.0	59.2	**72.5**
	Arena-Hard	4.5	17.6	8.5	**43.1**
	AlignBench v1.1	5.00	6.24	6.10	**7.60**
	Creative Writing v3	16.4	**51.1**	30.6	48.0
	WritingBench	4.03	5.42	5.61	**7.02**
Math & Text Reasoning	MATH-500	83.9	89.1	77.6	**93.4**
	AIME'24	28.9	**50.4**	10.7	48.3
	AIME'25	22.8	27.8	15.1	**36.8**
	ZebraLogic	4.9	37.1	30.3	**63.2**
	AutoLogi	19.1	63.4	61.6	**83.2**
Agent & Coding	BFCL v3	14.0	21.5	46.4	**56.6**
	LiveCodeBench v5	13.2	**42.5**	12.3	33.2
Multilingual Tasks	Multi-IF	13.3	27.0	36.1	**51.2**
	INCLUDE	21.9	34.5	35.9	**51.8**
	MMMLU 14 languages	27.3	40.1	43.1	**59.1**
	MT-AIME2024	12.4	13.2	7.8	**36.1**
	PolyMath	14.5	10.8	11.4	**25.2**
	MLogiQA	29.0	32.8	40.9	**56.0**

Table 20: **Comparison among Qwen3-1.7B / Qwen3-0.6B (Non-thinking) and other non-reasoning baselines. The highest and second-best scores are shown in bold and underlined, respectively.**

		Gemma-3 -1B-IT	Phi-4-mini	Qwen2.5-1.5B -Instruct	Qwen2.5-3B -Instruct	Qwen3-0.6B	Qwen3-1.7B
	Architecture	Dense	Dense	Dense	Dense	Dense	Dense
	# Activated Params	1.0B	3.8B	1.5B	3.1B	0.6B	1.7B
	# Total Params	1.0B	3.8B	1.5B	3.1B	0.6B	1.7B
General Tasks	MMLU-Redux	33.3	**67.9**	50.7	64.4	44.6	64.4
	GPQA-Diamond	19.2	25.2	29.8	**30.3**	22.9	28.6
	C-Eval	28.5	40.0	53.3	**68.2**	42.6	61.0
	LiveBench 2024-11-25	14.4	25.3	18.0	23.8	21.8	**35.6**
Alignment Tasks	IFEval strict prompt	54.5	**68.6**	42.5	58.2	54.5	68.2
	Arena-Hard	17.8	32.8	9.0	23.7	6.5	**36.9**
	AlignBench v1.1	5.3	6.00	5.60	6.49	5.60	**7.20**
	Creative Writing v3	**52.8**	10.3	31.5	42.8	28.4	43.6
	WritingBench	5.18	4.05	4.67	5.55	5.13	**6.54**
Math & Text Reasoning	MATH-500	46.4	67.6	55.0	67.2	55.2	**73.0**
	AIME'24	0.9	8.1	0.9	6.7	3.4	**13.4**
	AIME'25	0.8	5.3	0.4	4.2	2.6	**9.8**
	ZebraLogic	1.9	2.7	3.4	4.8	4.2	**12.8**
	AutoLogi	16.4	28.8	22.5	29.9	37.4	**59.8**
Agent & Coding	BFCL v3	16.3	31.3	47.8	50.4	44.1	**52.2**
	LiveCodeBench v5	1.8	10.4	5.3	9.2	3.6	**11.6**
Multilingual Tasks	Multi-IF	32.8	40.5	20.2	32.3	33.3	**44.7**
	INCLUDE	32.7	**43.8**	33.1	**43.8**	34.4	42.6
	MMMLU 14 languages	32.5	51.4	40.4	**51.8**	37.1	48.3
	MT-AIME2024	0.2	0.9	0.7	1.6	1.5	**4.9**
	PolyMath	3.5	6.7	5.0	7.3	4.6	**10.3**
	MLogiQA	31.8	39.5	40.9	39.5	37.3	**41.1**

Yang, A., et al. (2025). Qwen3 Technical Report. arXiv. https://doi.org/10.48550/arXiv.2505.09388.
https://huggingface.co/Qwen/Qwen3-0.6B (дата обращения: 16.03.2026).